IEEE Photonics Journal
An IEEE Photonics Society Publication

Open Access

All-Optical Ultrasound Transducer Using CNT-PDMS and Etalon Thin-Film Structure

Volume 7, Number 6, December 2015

Geonwook Yoo
Hyunmin Yoon
Jeongmin Heo
Ujwal Kumar Thakur
Hui Joon Park
Hyoung Won Baac
Junseok Heo, Member, IEEE

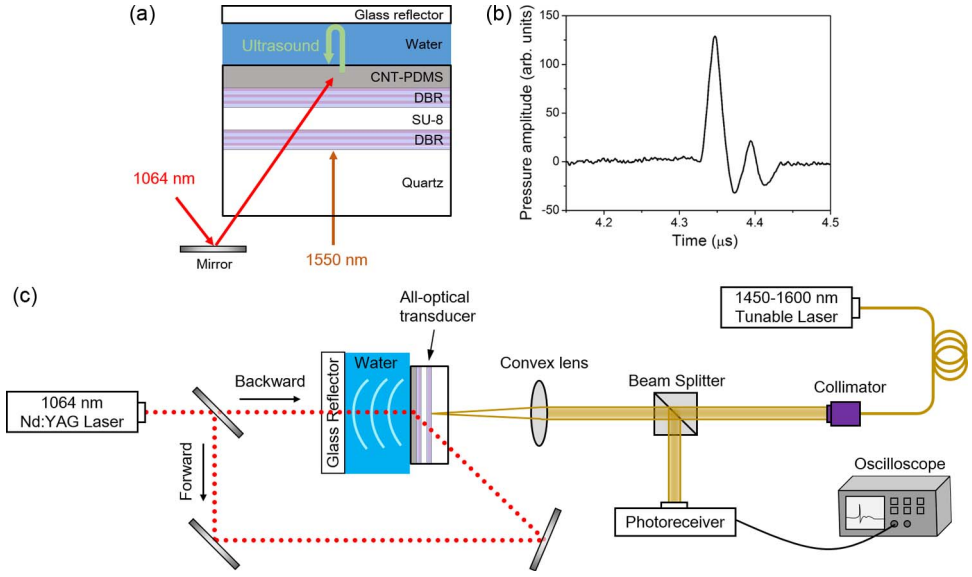

DOI: 10.1109/JPHOT.2015.2496862
1943-0655

All-Optical Ultrasound Transducer Using CNT-PDMS and Etalon Thin-Film Structure

Geonwook Yoo,[1] Hyunmin Yoon,[2] Jeongmin Heo,[3] Ujwal Kumar Thakur,[4] Hui Joon Park,[4] Hyoung Won Baac,[3] and Junseok Heo,[2] *Member, IEEE*

[1]Display Convergence Research Center, Korea Electronics Technology Institute, Seongnam 463-816, Korea
[2]Department of Electrical and Computer Engineering, Ajou University, Suwon 443-749, Korea
[3]School of Electronic and Electrical Engineering, Sungkyunkwan University, Suwon 440-746, Korea
[4]Division of Energy Systems Research, Ajou University, Suwon 443-749, Korea

DOI: 10.1109/JPHOT.2015.2496862

Manuscript received August 20, 2015; revised October 23, 2015; accepted October 28, 2015. Date of publication November 3, 2015; date of current version November 18, 2015. This work was supported in part by the Basic Science Research Program through the National Research Foundation of Korea (NRF) funded by the Ministry of Science, ICT, and Future Planning (NRF-2013R1A1A1058044) and in part by the Nano Material Technology Development Program through the NRF, funded by the Ministry of Science, ICT, and Future Planning (2009-0082580). H. W. Baac was supported by the Human Resources Development Program of the Korea Institute of Energy Technology Evaluation and Planning (KETEP) under Grant 20144030200580, funded by the Ministry of Trade, Industry, and Energy of the Korean Government. G. Yoo and H. Yoon contributed equally to this paper. Corresponding authors: H. W. Baac and J. Heo (e-mail: hwbaac@skku.edu; jsheo@ajou.ac.kr).

Abstract: Compared with conventional piezoelectric transductions, an all-optical high-frequency ultrasound (HFUS) transducer is a promising modality for high-resolution ultrasound imaging. We demonstrate an all-optical HFUS transducer by integrating a carbon nanotube–polydimethylsiloxane composite film with an etalon thin-film structure incorporating SiO_2/TiO_2 distributed Bragg reflectors and an SU-8 resonator. The optical and acoustic characteristics are investigated for two different configurations (forward and backward operation modes). The maximum amplitude of the pulse echo in backward mode is approximately twofold higher than that of the forward mode. This difference is contributed by the increased reflectance and the absorptive loss of the incident pulsed laser in the forward mode. The pulse echo from the transducer exhibits a broad frequency bandwidth of 27 MHz. Furthermore, the scalability of the 2-D all-optical transducer array is also evaluated by characterizing the optical properties of the etalon across an area of 0.1×0.2 mm^2. Our experimental results show that the proposed transducer is a promising candidate for high-resolution ultrasound imaging systems.

Index Terms: Ultrasound transducer, ultrasound detector, ultrasound transmitter, Fabry–Pérot interferometer, carbon nanotube.

1. Introduction

High-frequency ultrasound (HFUS) in the tens-of-megahertz range is highly useful for high-resolution endoscopy [1], intravascular imaging [2], and other medical imaging applications [3], [4]. Many of these applications require ultrasound systems with a small-size compact transducer capable of generating and detecting acoustic signals efficiently. However, for conventional transducers made of piezoelectric ceramics, it is challenging to fabricate microscale transducer elements and arrays, owing to electrical issues such as the impedance increasing with

a reduced element area [together with a decreasing signal-to-noise ratio (SNR)], element-to-element crosstalk, a lowered coupling factor, and electrical connections, all of which result in signal distortion and poor image quality [5].

All-optical HFUS transducers that optically generate and detect ultrasound can circumvent the limits imposed on existing transducers [6]. For HFUS generation, the photoacoustic effect can be used by irradiating with nanosecond laser pulses onto a thin-film transmitter that performs light absorption, heat conversion, and thermoacoustic generation of pulsed ultrasound. A variety of materials and structures such as metallic thin films [7]–[9], polymer composites with carbon nanotubes (CNTs) [10], carbon nanofibers [11], carbon black powders [12], and gold nanoparticles [13] have been studied to produce high-amplitude ultrasound output. For the optical detection of ultrasound, interferometric systems have been utilized to take advantage of highly sensitive optical resonance: for example, microring resonators [14]–[16], Fabry–Pérot etalons [17]–[19], and Mach–Zehnder interferometers [20], [21]. In particular, the Fabry–Pérot interferometer, such as Au/polymer/Au and Au/polymer/dielectric structures [17]–[19], is suitable for thin-film configuration. The compressible optical resonator between two reflecting mirrors sensitively responds to acoustic vibration and undergoes thickness modulation, leading to a shift in the resonance wavelength [8]. In all-optical transducers, the sensitivity of the transducer can be maintained in a decreasing active area because the detection area is optically defined on an order of microns without electrical connections. In addition, the optical generation of ultrasound would be achieved over the same element dimension. Such all-optical operation has been achieved by using a Fabry–Pérot etalon integrated with a transmitter layer [6], [19], [22], [23]. Hou *et al.* used an etalon as a detector with one of its mirrors fabricated by an array of Au nanostructure working as a transmitter [22]. Despite low optical absorption (~30%), it could successfully allow high-resolution imaging (19 μm in axial and 38 μm in lateral) due to high-frequency characteristics (center: 40 MHz, bandwidth: 57 MHz). A similar design but with black polydimethylsiloxane (PDMS) was used to improve the optical absorption [6]. An integrated structure of a polyimide film with an etalon has been also used, exhibiting a noise-equivalent pressure (NEP) of 3.3 kPa in the detector and a pressure output of 213 kPa with a 43-μm spot dimension at the transmitter [19]. In particular, the etalon performance in terms of NEP has been significantly improved by introducing a waveguide between two mirrors to reduce diffraction loss [23].

In this work, we demonstrate an all-optical HFUS transducer with a Fabry–Pérot etalon that consists of two (six pairs and three pairs of SiO_2/TiO_2) distributed Bragg reflectors (DBR), an SU-8 optical resonator, and a CNT-PDMS composite film transmitter on top of an etalon thin-film structure. Although the CNT-PDMS film has exhibited excellent transmitter performance in terms of high-frequency and high-amplitude pressure generation, it has not been utilized so far for all-optical ultrasound transducers. In our configuration, the SU-8 based optical resonator sandwiched between two DBR mirrors with the center of the stopband at 1550 nm results in multiple optical resonances at an approximately 1550-nm wavelength for acoustic sensing. This simultaneously exhibits low reflection (15%) at a 1064-nm wavelength, which should be an open window for pulsed photoacoustic excitation of the CNT-PDMS transmitter. Here, the CNTs can allow for heavy optical absorption (~100%) at a 1064-nm wavelength. We characterize the optical as well as acoustic performance of the proposed transducer for two different configurations (forward and backward operation modes) using a 1550-nm continuous-wave (CW) laser and a 1064-nm Nd:YAG pulsed laser. Finally, we evaluate the spatial uniformity of our etalon across a 0.1×0.2 mm^2 area in terms of resonance optical spectra, considering an application to a scanning all-optical transducer for a 2-D array operation.

2. Experimental

Fig. 1(a) and (b) show a cross-sectional schematic of the transducer with two different measurement configurations: forward mode and backward mode. Two modes were chosen to compare the performance of the transducer when the photoacoustic transmitter is excited through the etalon layer or directly excited from the water side without an obstruction layer. The fabrication

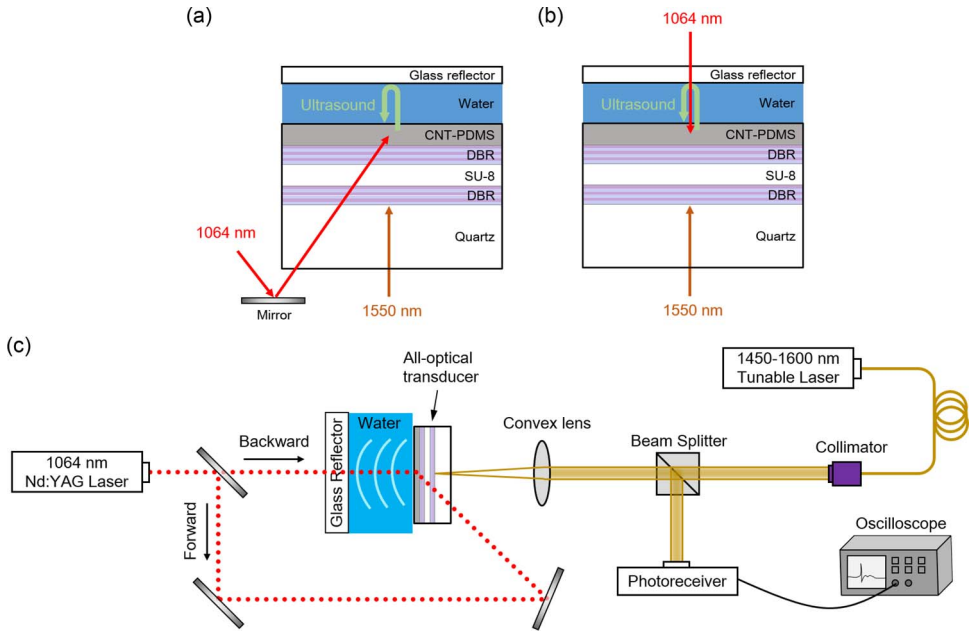

Fig. 1. Schematic illustration of the all-optical transducer with CNT-PDMS composite film layer and thin-film etalon incorporating two DBRs. The SU-8 resonator is presented with two characterization configurations: (a) forward mode and (b) backward mode. (c) Experimental setup for pulse-echo measurement with 1064-nm pulse laser for ultrasound generation in CNT-PDMS layer and tunable 1550-nm CW laser for detection in an etalon.

of the transducer begins with the deposition of alternating 240-nm-thick SiO_2 and 155-nm-thick TiO_2 on a quartz substrate by an electron beam evaporation process. A 15-μm-thick SU-8 polymer layer as an optical resonant cavity was then spin-coated and cured at 160 °C for 20 min. Spin-cast films were visually inspected under the microscope and showed no cracks or pinholes. The top DBR consisting of TiO_2 and SiO_2 was deposited in a similar way to the bottom DBR. Finally, a CNT-PDMS composite film with a thickness of 10–15 μm, acting as an ultrasound transmitter, was spin-coated on top of the top DBR.

An experimental setup for characterizing the optical and acoustic performances of the fabricated devices is illustrated in Fig. 1(c). An integrated all-optical transducer is mounted on a water tank. A 10-ns pulsed laser (1064-nm wavelength; Litron Lasers, U.K.) was used to excite the CNT-PDMS composite film. Two configurations, depending on the direction of the incident pulsed laser, were adopted for transducer characterization. In the forward mode, the pulsed laser was incident onto the transparent substrate side of the device at an angle of 40° [Fig. 1(a)], while in the backward mode, it was incident in a normal direction onto the top CNT-PDMS side [see Fig. 1(b)]. In both cases, the generated ultrasound was reflected back from a glass reflector positioned at 3 mm from the transducer and then detected by a 1550-nm CW probing beam through the etalon.

3. Results and Discussion

In our transducer configuration, the CNT-PDMS transmitter is placed on top of the etalon formed on a transparent substrate. For forward-mode operation, which is common for ultrasound imaging, a nanosecond-pulsed laser beam would be incident from the transparent side to the etalon and then the CND-PDMS composite film. This mode of operation requires high optical transmission through the etalon at a wavelength for photoacoustic excitation. Fig. 2(a) shows the reflection spectrum of the etalon detector measured by using a spectrophotometer. The reflectance at the fundamental (1064 nm) and the second harmonic (532 nm) wavelengths of the Nd:YAG

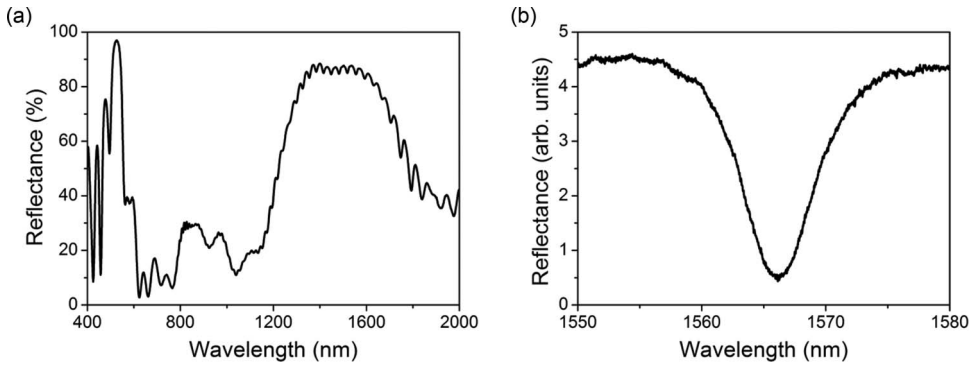

Fig. 2. (a) Reflection spectrum of the etalon consisting of three pairs and six pairs of SiO_2/TiO_2 layers with SU-8 in between. (b) Resonance profile of the etalon with a 15-μm-thick CNT-PDMS composite film in the range of tunable 1550-nm CW laser source.

pulsed laser are 15% and 96%, respectively. Our DBR design allows the etalon to have a high optical transmission at the 1064-nm wavelength, which is available to excite the CNT-PDMS transmitter. However, if a 532-nm wavelength is used for photoacoustic excitation, more than 96% of the laser beam would be reflected back by the DBR mirror before it reaches the transmitter.

Once the 1064-nm laser beam passes through the etalon, it is heavily absorbed by the CNT-PDMS film. Note that the CNT exhibits high intrinsic optical absorption over a broad spectral range from visible to IR wavelengths. This provides great flexibility in the DBR design because the optical design only considers how to achieve high reflection (specifically, at a 1550-nm wavelength) for interrogation of the sensor, while the wavelength for pulsed laser excitation and optical absorption can be easily chosen to be anywhere except the stopband of the DBRs. Moreover, the fundamental mode of the Nd:YAG laser is more favorable to excite the CNT-PDMS composite film so that any power loss associated with the second harmonic generation can be avoided. In Fig. 2(a), the spectrophotometer measurement was limited by the spot size of the probe beam $(0.8 \times 1.1\ \text{cm}^2)$ (i.e., averaging out the cavity resonance spectrum over the area), which is much larger than that of the 1550-nm CW laser beam (a diameter of 65 μm) used for acoustic sensing. We examined the resonance profile of the etalon coated with a CNT-PDMS composite film by sweeping a CW-tunable laser source from 1550 nm to 1580 nm and recording the optical reflection [Fig. 2(b)]. A resonance peak was located at a wavelength of 1566 nm with a full width at half maximum (FWHM) of 7.7 nm, which corresponds to a quality factor (Q) of 203 from $Q = \lambda_0/\Delta\lambda$, where λ_0 is the resonance wavelength and $\Delta\lambda$ is the FWHM [24].

Next, we performed a pulse-echo measurement for the two modes of operation according to the direction of the pulsed laser incidence, as illustrated in Fig. 1. Fig. 3(a) shows the measured pulse-echo signal in the forward operation mode. The distance between the all-optical transducer and the glass reflector was ~3.26 mm. This resulted in a round-trip temporal delay of $\sim$4.35 μs, which corresponded to 6.53 mm in distance. In the backward operation mode, the pulsed laser beam was directly focused on the CNT-PDMS layer from the top, interfaced with water, and thus, almost 100% of the pulsed laser energy was utilized for acoustic wave generation. The maximum amplitude of the measured pulse echo in this mode was approximately two folds higher than that of the forward mode, as shown in Fig. 3(b). This amplitude difference was also confirmed in the plot of peak pressure vs. pulsed laser fluence [see Fig. 3(c)].

The difference in the pulse-echo signal strength is mainly a result of the angled incidence of the pulsed laser in the forward mode as the stopband of the DBR shifted toward shorter wavelengths because of the additional in-plane wave vector. The estimated shift of the stopband is approximately 120 nm for an incident angle of 40° of the 1064-nm laser beam, which consequently increases the reflectance at 1064 nm to 35% [25]. In addition to the reflective loss mentioned above, another reason for the amplitude difference depending on the operation modes is

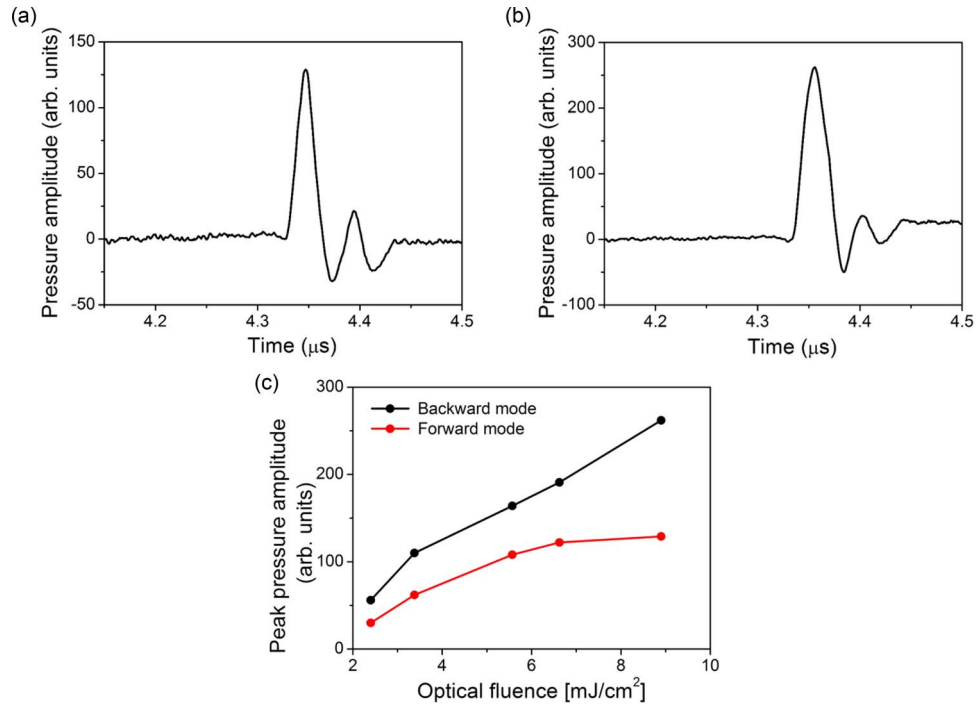

Fig. 3. Pulse-echo signal of the transducer measured in (a) forward and (b) backward modes. (c) Comparison of peak pressure amplitude for both measurement modes in response to pulsed laser fluence.

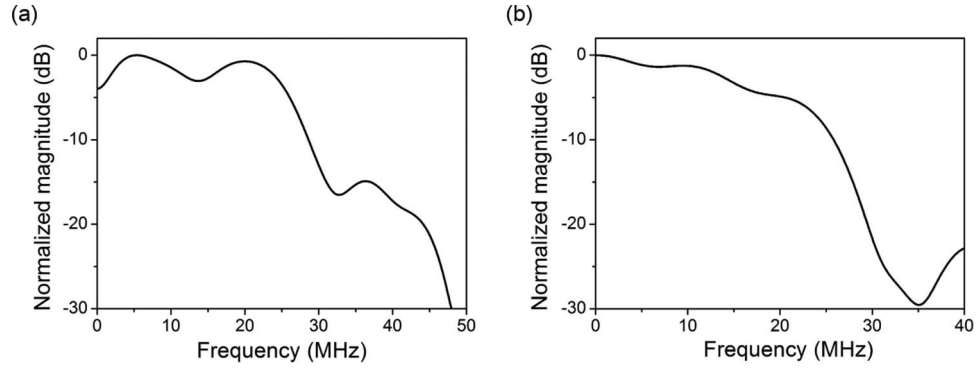

Fig. 4. Frequency spectra of the measured pulse echoes for (a) forward mode and (b) backward mode.

the absorptive loss when the incident pulsed laser goes through the 15-μm-thick etalon structure in the forward mode.

Fig. 4 shows the acoustic frequency spectra for the recorded pulse echoes. For both modes, the 6-dB frequency bandwidth was approximately 27 MHz. However, each spectral composition within the 6-dB bandwidth shows a relative difference, although the same CNT-PDMS transmitter was used for characterization. The forward-mode pulse echo has a spectral peak at a 20-MHz frequency whose magnitude is > 3 dB higher than the backward-mode pulse echo. By contrast, for the low-frequency region near dc, the spectral magnitude of the forward mode is less than that of the backward mode. This is consistent with the narrower pulse width (18.4 ns) of the forward-mode pulse echo as compared with that of the backward mode (26.1 ns) (see Fig. 3).

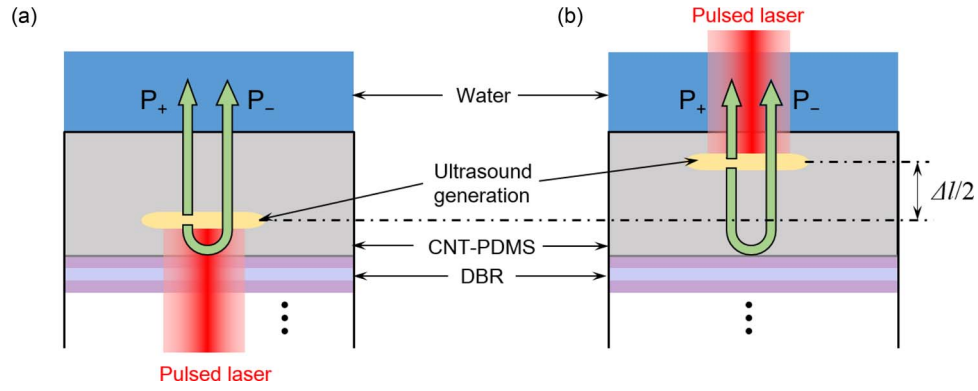

Fig. 5. Ultrasound pulse generation mechanism in (a) forward mode and (b) backward mode. The output pressure pulse from the transducer results from the sum of subpulses: the pulse directly propagating in the +z-direction (P_+), plus the back-propagating (P_-) and then reflected pulses. The final output pulse broadens as the acoustic path difference increases among these subpulses.

The spectral difference can be explained by the pulse generation mechanism in each mode that is associated with the location of optical absorption within the CNT-PDMS film (Fig. 5). First, we note that the depth of optical absorption for the CNT-PDMS film used here is on the order of several micrometers (i.e., the optical intensity drops to $1/e$), which is thinner than the CNT-PDMS film thickness ($\sim$15 μm). Therefore, during the forward-mode excitation, optical absorption occurs mostly at the bottom portion of the CNT-PDMS film interfaced with the top DBR mirror [Fig. 5(a)], while the absorption in the backward mode occurs at the top region of the CNT-PDMS interfaced with water [see Fig. 5(b)]. For both modes, the output pressure pulse from the transducer results from the sum of subpulses (see the arrows in Fig. 5) [26], i.e., the subpulse directly propagating in the +z-direction (P_+), plus the back-propagating and then reflected subpulses (P_-). Note that the back-propagating pulse is partially reflected and partially transmitted at every heterointerface, resulting in multiple subpulses. This means that the final output pulse broadens as the acoustic path difference increases among these subpulses. In the backward mode of excitation, where P_+ and P_- are simultaneously generated at the top portion of the CNT-PDMS film, the broadening of the output pulse significantly increases due to the elongated path (Δl) of P_- by the double passage across the CNT-PDMS film as compared to the forward mode (see Fig. 5). Such a generation mechanism could lead to a broader pulse width in the backward mode [see Fig. 3(b)] as well as a reduced magnitude over the high-frequency range.

The spatial uniformity of the transducer performance is important when 2-D array operation is considered. This is because the uniformity leads to consistent acoustic performance of individual elements that are optically defined and interrogated by scanning a probe laser beam. In our stacked structure, spatial nonuniformity can result from surface roughness and thickness variations of the DBR mirrors and SU-8 resonator [8]. We confirmed the uniformity by spatially characterizing the optical resonance profiles of the etalon over an area of 0.1×0.2 mm^2. We randomly chose four points across the device area and measured the optical resonance spectrum three times to obtain an average profile for each point. Fig. 6 shows that the variation of the resonance peak ranges from 1566.0 nm to 1566.4 nm, depending on each measured location. This minimal variation guarantees that the consistent transduction in the etalon is available over the area.

Further improvements to our proposed all-optical transducer can be accomplished in several ways. First, by increasing the reflectivity of the DBR mirror at the probe beam wavelength, the sensitivity of our etalon detector would be enhanced because the *Q*-factor of a resonator increases with the mirror's reflectivity. The lateral confinement of the cavity by the mesa definition can be also considered so that the divergence of light in the cavity is minimized, leading to a better detection of ultrasound [23]. Although higher pulse-echo amplitude was obtained in the

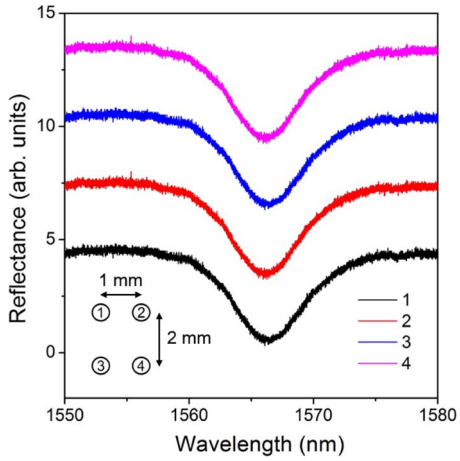

Fig. 6. Spatial variation of the etalon's optical resonance profiles across an area of 1×2 mm^2.

backward mode owing to the direct excitation of the pulsed laser, the pulse-echo strength in the forward mode can be further enhanced by rearranging the incidence of the 1064-nm pulsed laser beam. A normal incidence for the pulsed laser beam would be achieved by using a beam splitter that combines and delivers two laser beams for acoustic sensing (1550-nm wavelength) and photoacoustic excitation (1064 nm) in the same direction [22]. Furthermore, the DBR mirrors can be apodized by varying the thickness of each layer in the DBR so that the reflections of higher-order and side-lobe modes are suppressed, improving the transmission of the pulsed laser exciting the CNT-PDMS.

4. Conclusion

We demonstrated an all-optical HFUS transducer consisting of a CNT-PDMS composite film on top of an etalon thin-film structure. The etalon, acting as a detector, comprises two DBR mirrors and an SU-8 resonator. Optical sensing of ultrasound was achieved by using a 1550-nm CW laser. The CNT-PDMS transmitter was used for the efficient generation of high-frequency pulsed ultrasound. The broad optical absorption of the CNT allowed for photoacoustic excitation by a 1064-nm wavelength. The pulse echo from the transducer exhibited a broad frequency bandwidth of 27 MHz owing to the advantages of optical generation and detection. The etalon showed a resonance peak at 1566 nm with a Q-factor of 203, and the resonance peak variation was minimal within a range of < 0.5 nm over an area of 0.1×0.2 mm^2. We expect that the optical and acoustic performances can be further improved by optimizing the DBR mirror and resonator design. The demonstrated transducer offers a promising approach for developing all-optical HFUS transducers applicable to high-resolution ultrasound imaging.

References

[1] F. E. Silverstein *et al.,* "Experimental evaluation of an endoscopic ultrasound probe: In vitro and in vivo canine studies," *Gastroenterology*, vol. 96, no. 4, pp. 1058–1062, Apr. 1989.
[2] R. A. White *et al.,* "Vascular imaging before, during and after endovascular repair," *World J. Surg.*, vol. 20, no. 6, pp. 622–629, Jul. 1996
[3] D. J. Coleman *et al.,* "High-resolution ultrasonic imaging of the posterior segment," *Ophthalmol.*, vol. 111, no. 7, pp. 1344–1351, Jul. 2004.
[4] F. S. Foster *et al.,* "A new ultrasound instrument for in vivo microimaging of mice," *Ultrasound Med. Biol.*, vol. 28, no. 9, pp. 1165–1172, Sep. 2002.
[5] J. M. Cannata, J. A. Williams, Q. Zhou, T. A. Ritter, and K. K. Shung, "Development of a 35-MHz piezo-composite ultrasound array for medical imaging," *IEEE Trans. Ultrason., Ferroelectr., Freq. Control*, vol. 53, no. 1, pp. 224–236, Jan. 2006.
[6] Y. Hou, S. Ashkenazi, S.-W. Huang, and M. O'Donnell, "An integrated optoacoustic transducer combining etalon and black PDMS structures," *IEEE Trans. Ultrason., Ferroelectr., Freq. Control*, vol. 55, no. 12, pp. 2719–2725, Dec. 2008.

[7] R. J. von Gutfeld and R. L. Melcher, "20 MHz acoustic waves from pulsed thermoelastic expansions of constrained surfaces," *Appl. Phys. Lett.*, vol. 30, no. 6, pp. 257–259, Apr. 1977.
[8] P. C. Beard, F. Perennes, and T. N. Mills, "Transduction mechanisms of the Fabry–Perot polymer film sensing concept for wideband ultrasound detection," *IEEE Trans. Ultrason., Ferroelectr., Freq. Control*, vol. 46, no. 6, pp. 1575–1582, Nov. 1999.
[9] X. Wang and X. Xu, "Thermoelastic wave induced by pulsed laser heating," *Appl. Phys. A*, vol. 73, no. 1, pp. 107–114, Jul. 2001.
[10] H. W. Baac *et al.,* "Carbon nanotube composite optoacoustic transmitters for strong and high frequency ultrasound generation," *Appl. Phys. Lett.*, vol. 97, no. 23, Dec. 2010, Art. ID 234104.
[11] B. Hsieh *et al.,* "A laser ultrasound transducer using carbon nanofibers-polydimethylsiloxane composite thin film," *Appl. Phys. Lett.*, vol. 106, no. 2, Jan. 2015, Art. ID 021902.
[12] E. Biagi, F. Margheri, and D. Menichelli, "Efficient laser-ultrasound generation by using heavily absorbing films as targets," *IEEE Trans. Ultrason., Ferroelectr., Freq. Control*, vol. 48, no. 6, pp. 1669–1680, Nov. 2001
[13] Y. Hou, J. Kim, S. Ashkenazi, M. O'Donnell, and J. Guo, "Optical generation of high frequency ultrasound using two-dimensional gold nanostructure," *Appl. Phys. Lett.*, vol. 89, no. 9, Aug. 2006, Art. ID 093901.
[14] A. Maxwell *et al.,* "Polymer microring resonators for high-frequency ultrasound detection and imaging," *IEEE J. Sel. Topics Quantum Electron.*, vol. 14, no. 1, pp. 191–197, Feb. 2008.
[15] T. Ling, S.-L. Chen, and L. J. Guo, "High-sensitivity and wide-directivity ultrasound detection using high Q polymer microring resonators," *Appl. Phys. Lett.*, vol. 98, no. 20, May 2011, Art. ID 204103.
[16] H. Li, B. Dong, Z. Zhang, H. F. Zhang, and C. Sun, "A transparent broadband ultrasonic detector based on an optical micro-ring resonator for photoacoustic microscopy," *Sci. Rep.*, vol. 4, Mar. 2014, Art. ID 4496.
[17] J. D. Hamilton, T. Buma, M. Spisar, and M. O'Donnell, "High frequency optoacoustic arrays using etalon detection," *EEE Trans. Ultrason., Ferroelectr., Freq. Control*, vol. 47, no. 1, pp. 160–169, Jan. 2000.
[18] S. Ashkenazi, Y. Hou, T. Buma, and M. O'Donnell, "Optoacoustic imaging using thin polymer etalon," *Appl. Phys. Lett.*, vol. 86, no. 13, Mar. 2005, Art. ID 134102.
[19] C. Sheaff and S. Ashkenazi, "Characterization of an improved polyimide-etalon all-optical transducer for high-resolution ultrasound imaging," *EEE Trans. Ultrason., Ferroelectr., Freq. Control*, vol. 61, no. 7, pp. 1223–1232, Jul. 2014.
[20] G. Paltauf, R. Nuster, M. Haltmeier, and P. Burgholzer, "Photoacoustic tomography using a Mach-Zehnder interferometer as an acoustic line detector," *Appl. Opt.*, vol. 46, no. 16, pp. 3352–3358, May 2007.
[21] D. Gallego and H. Lamela, "High-sensitivity ultrasound interferometric single-mode polymer optical fiber sensors for biomedical applications," *Opt. Lett.*, vol. 34, no. 12, pp. 1807–1809, Jun. 2009.
[22] Y. Hou *et al.,* "Broadband all-optical ultrasound transducers," *Appl. Phys. Lett.*, vol. 91, no. 7, Aug. 2006, Art. ID 073507.
[23] M. A. Tadayon, M.-E. Baylor, and S. Ashkenazi, "Polymer waveguide Fabry–Perot resonator for high-frequency ultrasound detection," *EEE Trans. Ultrason., Ferroelectr., Freq. Control*, vol. 61, no. 12, pp. 2132–2138, Dec. 2014.
[24] J. T. Verdeyen, *Laser Electronics*, 3rd ed. Englewood Cliffs, NJ, USA: Prentice-Hall, 1995.
[25] J. Heo, S. Jahangir, B. Xiao, and P. Bhattacharya, "Room-temperature polariton lasing from GaN nanowire array clad by dielectric microcavity," *Nano Lett.*, vol. 13, no. 6, pp. 2376–2380, May 2013.
[26] V. E. Gusev and A. A. Karabutov, *Laser Optoacoustics*. New York, NY, USA: AIP, 1993.